Mass distribution studies in ^{20}Ne + ^{232}Th reaction

Suparna Sodaye,* R. Tripathi, K. Sudarshan, and R. Guin
Radiochemistry Division, Bhabha Atomic Research Centre, Trombay, Mumbai 400 085, India
(Received 27 February 2013; published 17 April 2013)

Fission product mass distributions were measured in ^{20}Ne + ^{232}Th reaction at E_{lab} = 142.5 and 114 MeV using recoil catcher technique followed by off-line γ-ray spectrometry. Fission products formed predominantly in complete fusion fission (CFF) or transfer-induced fusion fission (TF) were distinguished based on their A/Z. Two groups of fission products that centered around A/Z for CFF and TF were observed. Mass distributions for CFF and TF were obtained after applying corrections for charge distribution using parameters appropriate for CFF and TF. A symmetric mass distribution was observed for CFF. For TF, mass distribution was observed to be asymmetric, indicating a significant role of shell effect owing to the lower excitation energy of the fissioning system. Variance of mass distribution at E_{lab} = 142.5 MeV was calculated using the random neck rupture model (RNRM). The scission-point elongation parameter obtained by RNRM calculations was higher compared to that obtained from the liquid drop model.

DOI: 10.1103/PhysRevC.87.044610 PACS number(s): 25.70.Jj, 25.85.Ge, 24.75.+i

I. INTRODUCTION

Mass distribution in fission provides information about the potential energy landscape of the fissioning nucleus and the mechanism involved [1,2]. A large amount of experimental data on the mass distribution in nuclear fission has been generated over the years. The main interest in the medium-energy heavy-ion-induced fission is to study the effect of entrance channel parameters, namely, projectile energy, angular momentum, and entrance channel mass asymmetry on the fission process. Experimental formation cross sections of fission products can have contributions from several reaction processes, thereby complicating the mass distributions and the interpretation of the results. The mass distributions have contributions from mainly three reaction mechanisms: complete fusion fission (CFF), noncompound nucleus fission (NCF), and transfer-induced fission (TF). In CFF, fission occurs from a fully equilibrated compound nucleus formed by fusion of the projectile with the target nucleus. Heavy fissioning systems are characterized by a small fission barrier as well as saddle-point elongation. For such systems, the composite system formed in many collision trajectories may undergo NCF. The NCF involves full momentum transfer as in CFF, but fission occurs before the formation of a fully equilibrated fissioning system. The signatures of NCF are broader or asymmetric mass distribution [2–12] and higher anisotropy of the fission fragment angular distribution [13–16] compared to that for compound nucleus fission. Transfer-induced fission involves partial momentum transfer owing to the capture of a part of the projectile by the target. This is followed by the formation of a fully equilibrated fissioning system, though lighter than the compound nucleus for CFF and having different A/Z. In on-line experiments, full momentum transfer events leading to CFF and NCF, if present, can be delineated from TF events by folding angle measurement. In the off-line radiochemical measurements, the effects of TF on fission observables such as mass and angular distributions can be discerned based on A/Z of the fission products [17–20]. Contribution from TF would lead to an increase in the variance of mass distribution because A/Z of the fissioning nucleus would be different in CFF and TF. Hinde *et al*. [21] observed that the fission fragment mass distribution in 105- and 120-MeV ^{19}F + ^{232}Th reactions is not symmetric and attributed this to the presence of transfer fission component.

Various models have been used to explain the CFF mass distribution. The statistical saddle-point [22] and scission-point [23] models, though, qualitatively explained CFF mass distribution; they failed on a quantitative scale. The random neck rupture model (RNRM) has been successful in explaining the variance of the mass distribution in a large number of fissioning systems [24,25]. According to this model, exit channel fission observables are governed by the pre-scission shape. In this model, elongation of the pre-scission shape is a variable parameter which can be fixed by reproducing the experimental fragment/product mass distribution and kinetic energies. In our earlier studies [26–28], elongation parameters for scission-point shapes were determined using RNRM for fissioning systems spanning a wide range of fissility. A comparison of the elongation of the pre-scission shape obtained from RNRM with those obtained from the liquid drop model (LDM) scission criterion [29], based on LDM potential energy minimization, showed that RNRM shapes were more elongated. The ratio of elongation parameters was nearly a constant factor of about ∼1.76, though; a small systematic deviation was observed for highly fissile systems [26,27]. This was possibly attributable to the contribution from multichance fission and TF.

Thus, study of the effects of contribution from TF is important for understanding the heavy-ion fusion-fission mechanism and testing the theoretical models of fission mass distribution in heavy fissioning systems. In the present work, formation cross sections of fission products were measured by an off-line radiochemical method in ^{20}Ne + ^{232}Th reactions at E_{lab} = 142.5 and 114 MeV. This reaction would produce a highly fissile system which would have significant contribution

*suparna@barc.gov.in

from various noncompound processes. Fission product mass distributions were obtained from experimental yields of fission products after correcting for the charge distribution appropriate for CFF and TF. The variance of CFF mass distribution was calculated using RNRM and the elongation of the scission-point shape was compared with that obtained from the LDM scission-point criterion [29]. From the TF mass distribution, an estimate of the contribution from TF fission was obtained.

II. EXPERIMENTAL DETAILS

Experiments were carried out at Variable Energy Cyclotron Centre, Kolkata, India. Two irradiations were carried out to obtain the mass distribution at $E_{\rm lab} = 142.5$ and 114 MeV. For the first irradiation, a target assembly consisting of a self-supporting thorium target (3.08 mg/cm^2) and a thick aluminum catcher foil having thickness 6.75 mg/cm^2 in the forward direction was bombarded with a 145-MeV ^{20}Ne beam. Owing to the beam energy degradation in the target, average energy at the center of the target was 142.5 MeV. Irradiation was carried out for about 8 h. To determine the mass distribution at $E_{\rm lab} = 114$ MeV, a target catcher assembly consisting of a self-supporting thorium target having thickness 1.9 mg/cm^2 and two aluminum catcher foils of thickness 6.75 mg/cm^2 (one in the backward direction and the other in the forward direction were bombarded with a 145-MeV ^{20}Ne beam, so that the beam energy was 114 MeV at the center of the target. The durations of irradiation at the lower beam energy was about 13 h.

After irradiation, target and catcher foils were separately assayed for the γ-ray activity of the fission products using a high-purity germanium detector coupled to a multichannel analyzer. The activities of the fission products and ERs were corrected for the decay after irradiation. The unambiguous detection of fission products was carried out by matching half-lives and energies of the γ rays. The nuclear data of the radionuclides studied in the present work, namely, half-lives, γ-ray energies (E_γ), and abundances (I_γ), are given in Table I [30,31]. The γ-ray spectra of the fission products were analyzed to determine the peak areas of their characteristic γ rays using the PHAST software developed at the Electronics Division, Bhabha Atomic Research Centre [32]. The peak areas under the characteristic γ-ray peaks were used to obtain "end of irradiation activities (A)" of the fission products which were used to obtain their formation cross sections (σ) using the standard activation equation

$$\sigma = \frac{A}{N\phi(1 - e^{-\lambda T_{\rm irr}})a_\gamma \varepsilon_\gamma}, \qquad (1)$$

where, N is the number of target atoms per unit area, ϕ is the average number of beam particles incident on the target per unit time, λ is the decay constant of the fission product/evaporation residue, a_γ is the emission probability of γ ray with energy E_γ, and ε_γ is the full energy detection efficiency at energy E_γ. The formation cross sections of the fission products were used to obtain fission product mass distribution after correcting for the charge distribution.

TABLE I. Decay data of fission products and evaporation residues used in the present work, taken from Refs. [30,31].

Nuclide	Half-life	E_γ (keV)	I_γ
^{78}As	1.51 h	613.9	54.0
^{85}Kr^m	4.48 h	151.2	75.0
^{87}Kr	76.3 min	402.6	49.6
^{88}Kr	2.84 h	196.3	26.3
^{89}Rb	15.4 min	1248.1	46.7
^{91}Sr	9.63 h	749.8	23.6
^{92}Sr	2.71 h	1383.9	90.0
^{93}Y	10.18 h	266.9	7.3
^{94}Y	18.7 min	918.8	56.0
^{95}Zr	64.02 days	756.7	54.5
^{97}Zr	16.74 h	743.4	92.6
^{97}Nb	72.1 min	657.9	98.5
^{98}Nb	51.3 min	787.4	93.0
^{99}Mo	65.94 h	140.5	90.7
^{103}Ru	39.25 days	497.1	89.5
^{104}Tc	18.4 min	358.0	89.0
^{105}Ru	4.44 h	724.2	46.7
^{105}Rh	35.36 h	318.9	19.2
^{107}Rh	21.7 min	302.8	66.0
^{111}Pd^m	5.5 h	172.2	33.5
^{111}Ag	7.45 days	342.1	6.7
^{112}Pd	21.05 h	617.4	50.0
^{112}Ag	3.14 h	617.4	42.5
^{113}Ag^g	5.37 h	298.6	10.0
^{116}In^m	54.15 min	1293.5	84.4
^{117}Cd^m	3.36 h	158.6	109.0
^{117}Cd^g	2.49 h	273.3	27.9
^{120}Sb	5.76 days	197	88.0
^{122}Sb	2.72 days	564	70.8
^{124}Sb	60.2 days	602.7	98.4
^{125}Xe	16.9 h	188.4	54.0
^{126}I	13.02 days	388.6	32.2
^{126}Sb^g	12.46 days	414.8	83.2
^{127}Sb	3.85 days	685.7	36.6
^{127}Xe^g	36.41 days	202.9	68.3
^{128}I	25 min	442.9	16.0
^{130}I^g	12.36 h	536	99.0
^{131}I	8.02 days	364.5	81.7
^{132}Te	3.204 days	228.2	88.1
^{132}I^m	1.387 h	772.6	14.0
^{133}I^g	20.8 h	529.9	87.0
^{133}Ba	38.9 h	276.1	17.5
^{134}Cs^m	2.91 h	127.5	12.6
^{134}I	52.5 min	884	64.9
^{136}Cs	13.16 days	818.5	99.7
^{138}Cs	33.41 min	462.8	30.7
^{139}Ba	83.06 min	165.8	23.6
^{140}La	1.68 day	487	45.5
^{140}Ba	12.75 days	537.3	24.4
^{141}Ce	32.5 days	145.4	48.2
^{142}La	91.1 min	641.2	47.4
^{150}Pm	2.68 h	333.9	68.0
^{232}Pa	1.31 days	969.3	41.6
^{233}Pa	26.97 days	312.2	38.6

III. RESULTS AND DISCUSSION

A. Mass distribution studies at 142.5 MeV in ^{20}Ne + ^{232}Th reaction

At beam energy of 142.5 MeV, the experimentally determined cross sections correspond to the fission products collected in the forward catcher foil and target. To arrive at the total formation cross sections of fission products, correction factors were required for the fragments emitted in the backward direction. For this correction, forward-to-backward ratios for fission products were calculated using standard kinematic equations with fission fragment kinetic energies obtained using the prescription of Rossner *et al.* [33]. Forward-to-backward ratios were calculated for fission following full momentum transfer events. Fission fragment masses were transformed into the corresponding product masses after correcting for the neutrons evaporated in the fission process, which were calculated using the prescription of Kozuline *et al.* [34]. The number of evaporated neutrons was apportioned according to the fission fragment mass ratios. From the "forward to backward ratio," the correction factors for the emission of fission products in the backward hemisphere were calculated. The plot of "correction factor (c)" vs fission product mass number was fitted to a third-order polynomial ($c = 2.25003 - 0.00433\ A + 3.58\ e^{-5}\ A^2 - 1.53e^{-7}\ A^3$), which was used to correct the experimental cross sections of fission products for backward emission. Formation cross sections of 51 fission products, obtained in ^{20}Ne + ^{232}Th reaction at $E_{\rm lab} = 142.5$ MeV, are given in Table II. The independent and cumulative cross sections are marked by "I" and "C", respectively in the table. The uncertainties on the formation cross sections are quoted at the 1σ level.

To obtain the mass distribution, formation cross sections of the fission products have to be corrected for the charge distribution. The yield $Y(A)$ of a mass chain "A" is calculated using the independent $IN(A,Z)$ or cumulative $CU(A,Z)$ cross sections of the fission product with mass A and atomic number Z using the equations

$$Y(A) = IN(A,Z)/FIY(A,Z), \quad (2)$$

$$Y(A) = CU(A,Z)/FCY(A,Z), \quad (3)$$

where $FIY(A,Z)$ and $FCY(A,Z)$ are the fractional independent and cumulative yields, respectively, of the measured fission product having mass number A and atomic number Z. $FIY(A,Z)$ and $FCY(A,Z)$ are given by the equations

$$FIY(A,Z) = \frac{1}{\sqrt{2\pi\sigma_z^2}} \int_{Z-0.5}^{Z+0.5} e^{-(Z-Z_p)^2/2\sigma_z^2} dZ, \quad (4)$$

$$FCY(A,Z) = \frac{1}{\sqrt{2\pi\sigma_z^2}} \int_{-\infty}^{Z+0.5} e^{-(Z-Z_p)^2/2\sigma_z^2} dZ, \quad (5)$$

where σ_Z and Z_p are the width and most probable charge, respectively, for the isobaric yield distribution. Thus, calculation of the mass yield for a mass chain with mass number A from the experimentally determined yield of a fission product $[Y(A)]$ requires the information about the Z_p and σ_Z of the isobaric yield distribution for the mass chain with mass number A.

TABLE II. Formation cross section of fission products and evaporation residues produced in the ^{20}Ne + ^{232}Th reaction at beam energies of 142.5 and 114 MeV. Measured cross sections of fission products were either cumulative (C) or independent (I) as mentioned in the table.

Nuclide	Cross section (mb)	
	142.5 MeV	114 MeV
^{78}As	3.87 ± 1.25 (C)	
^{85}Kr^{m}	6.47 ± 1.36 (C)	
^{87}Kr	8.66 ± 1.75 (C)	2.70 ± 0.85 (C)
^{88}Kr	8.58 ± 1.04 (C)	
^{89}Rb	11.97 ± 3.98 (C)	
^{91}Sr	15.80 ± 3.58 (C)	2.94 ± 0.56 (C)
^{92}Sr	12.81 ± 1.56 (C)	2.91 ± 1.21 (C)
^{93}Y	15.06 ± 1.75 (C)	
^{94}Y	9.43 ± 2.70 (C)	
^{95}Zr	21.50 ± 2.90 (C)	4.57 ± 0.82 (C)
^{97}Zr	16.07 ± 0.42 (C)	3.42 ± 0.33 (C)
^{97}Nb	12.42 ± 1.19 (C)	
^{98}Nb	13.06 ± 1.53 (C)	
^{99}Mo	29.82 ± 4.13 (C)	4.84 ± 0.31 (C)
^{103}Ru	30.87 ± 9.94 (C)	4.12 ± 0.40 (C)
^{104}Tc	14.31 ± 2.59 (C)	
^{105}Ru	24.21 ± 1.57 (C)	
^{105}Rh	30.10 ± 3.12 (C)	5.53 ± 0.98 (C)
^{107}Rh	23.33 ± 3.06 (C)	
^{111}Pd^{m}	8.67 ± 1.72 (I)	3.25 ± 0.79 (I)
^{111}Ag	32.85 ± 6.17 (C)	14.6 ± 3.0 (C)
^{112}Pd	19.84 ± 1.35 (C)	
^{112}Ag	13.91 ± 0.39 (I)	
^{113}Ag^{g}	27.92 ± 12.00 (C)	
^{116}In^{m}	12.84 ± 2.23 (I)	
^{117}Cd^{g}	19.47 ± 1.55 (I)	2.02 ± 0.29 (I)
^{120}Sb	5.37 ± 1.16 (I)	
^{122}Sb	15.22 ± 2.08 (I)	1.60 ± 0.23 (I)
^{124}Sb	16.11 ± 2.39 (I)	
^{125}Xe	0.45 ± 0.13 (I)	
^{126}I	12.77 ± 0.79 (I)	1.24 ± 0.21 (I)
^{126}Sb^{g}	5.41 ± 0.26 (I)	1.22 ± 0.15 (I)
^{127}Sb	5.37 ± 1.38 (C)	1.66 ± 0.64 (C)
^{127}Xe^{g}	4.31 ± 1.66 (I)	
^{128}I	8.80 ± 3.85 (I)	
^{130}I^{g}	7.68 ± 1.08 (I)	1.43 ± 0.18 (I)
^{131}I	13.39 ± 0.41 (C)	3.07 ± 1.07 (C)
^{132}Te	5.82 ± 0.71 (C)	1.70 ± 0.15 (C)
^{132}I^{m}	4.74 ± 0.58 (I)	2.39 ± 0.25 (I)
^{133}I^{g}	6.92 ± 0.53 (C)	
^{133}Ba	6.03 ± 0.94 (I)	
^{134}Cs^{m}	9.18 ± 3.72 (I)	
^{134}I	7.97 ± 1.95 (C)	
^{136}Cs	5.02 ± 0.61 (I)	1.20 ± 0.21 (I)
^{138}Cs	8.14 ± 3.14 (C)	
^{139}Ba	11.19 ± 2.31 (C)	
^{140}La	8.81 ± 2.63 (C)	
^{140}Ba	7.19 ± 0.83 (C)	2.41 ± 0.30 (C)
^{141}Ce	23.36 ± 0.98 (C)	5.33 ± 0.64 (C)
^{142}La	6.37 ± 2.07 (C)	
^{150}Pm	4.02 ± 0.59 (I)	
^{232}Pa	21.70 ± 0.66	7.31 ± 0.67
^{233}Pa	33.42 ± 1.13	24.31 ± 1.01

Ideally, independent yields of at least three members in the isobaric chain are required to obtain these charge distribution parameters. However, in general, it is difficult to measure three independent yields in an isobaric chain and an alternative approach is generally used to obtain the charge distribution parameters as discussed in the next section.

1. Determination of charge distribution parameters

Isotopic yield distributions of the elements formed in fission can be used to extract the charge distribution parameters. In the present study, this method was used to find the charge distribution parameters using the experimentally determined independent yields of Sb (^{120,122,124,126}Sb) isotopes in the forward catcher foil. As for most of the Sb isotopes, the cross section of high-spin isomer was measured or the high-spin isomer completely decayed to the measured low-spin isomer through IT, the measured yields of the Sb isotopes were approximated as the total cross section of the respective isotopes. The isotopic yield distribution of Sb isotopes was fitted to a Gaussian function to obtain the width (σ_A) and most probable mass (A_p):

$$IN(A, Z) = \frac{Y(Z)}{\sqrt{2\pi\sigma_A^2}} e^{-\left[\frac{(A-A_p)^2}{2\sigma_A^2}\right]}. \quad (6)$$

The isotopic yield distribution for Sb isotopes along with fitted curve is shown in Fig 1. The values of σ_A and A_p were obtained as 1.93 ± 0.28 and 123.00 ± 0.01, respectively. The uncertainties quoted on these parameters are fitting errors. From the value σ_A, width of isobaric charge distributions σ_Z [$= \sigma_A/(A/Z)_p$] was obtained as 0.80 ± 0.12, which was used for the charge distribution correction of the experimental yield of fission products. The value of σ_Z determined in the present work was found be comparable with the σ_Z value of 0.84 as obtained in ^{11}B + ^{232}Th [35]. Based on unchanged charge distribution (UCD) hypothesis, the most probable charge Z_p for a particular mass chain with mass number A obtained as

$$Z_p(A) = A^* \left(\frac{Z}{A}\right)_p, \quad (7)$$

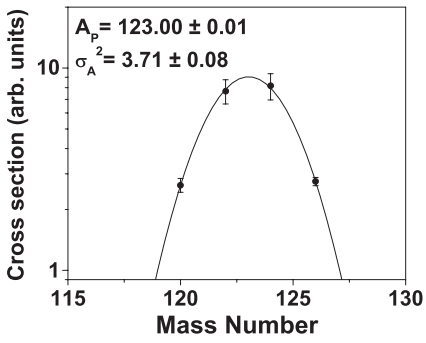

FIG. 1. Plot of yields of Sb isotopes in the forward catcher foil at E_{lab} = 142.5 MeV. The solid line is a Gaussian fit to the data. Variance and most probable mass obtained from the fit are also given in the figure. The quoted uncertainty is fitting error.

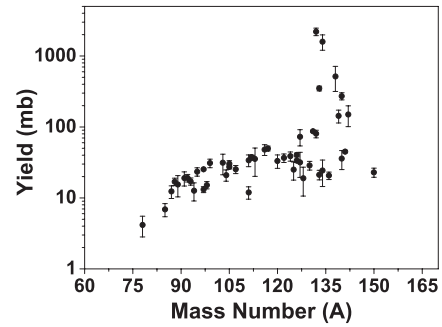

FIG. 2. Plot of mass yields obtained by correcting the experimental yields of fission products for the charge distribution using the charge distribution parameters for CFF.

with $(A/Z)_p$ calculated using the equation

$$(A/Z)_p = \frac{A_{cn} - \nu_T}{Z_{cn}}, \quad (8)$$

where, A_{cn} and Z_{cn} are the mass and atomic number, respectively, of the compound nucleus. ν_T is the average number of neutrons emitted during the fission process, which was calculated using the prescription of Kozuline *et al.* [34]. The calculated value of ν_T was 10.3. Z_p values for various mass chains obtained using $(A/Z)_p$ from Eq. (8) were used for the charge distribution correction using Eq. (4) or Eq. (5).

2. Mass distribution at E_{lab} = 142.5 MeV

The mass distribution obtained after charge distribution correction is plotted in Fig. 2. Most of the products, formed by CFF, fall on a Gaussian distribution. An unusually high yield of some of the products in the higher mass region (A = 132–143), obtained after charge distribution correction, indicate that the charge distribution parameters corresponding to CFF are not valid for these fission products. These products may have contribution from transfer fusion fission (TF), where the fissioning target-like nucleus has higher (A/Z) compared to that for the CFF. The experimentally measured fission products in the heavy-mass region are close to β stability valley, which shifts to higher A/Z with increasing mass. Therefore, these products are expected to have substantial contribution from TF for which the fissioning system is having higher A/Z. Dominant contribution from TF to fission products with higher A/Z was further confirmed from the plot of the mass yields (obtained after charge distribution correction) vs A/Z of the corresponding fission products as shown in Fig. 3. A systematic increase in the mass yields with increasing A/Z can be seen beyond 2.47, suggesting dominant contribution from TF to the fission products with $A/Z > 2.47$. A plot of independent or nearly independent (fission products at the lower end of the isobaric yield distribution) yields of fission products (^{117}Cd, ^{116}In, ^{112}Ag, ^{132}Te, ^{136,138}Cs, ^{133,140,141}Ba, ^{126,130g,132m,133g,134}I, ^{120,122,124,126}Sb) as a function of their A/Z is shown in Fig. 4. Solid lines in this figure are guides for the eye. Two separate groups of fission products arising from the CFF (centered at lower A/Z) and TF (centered at higher A/Z) can be seen in this figure. The left arrow

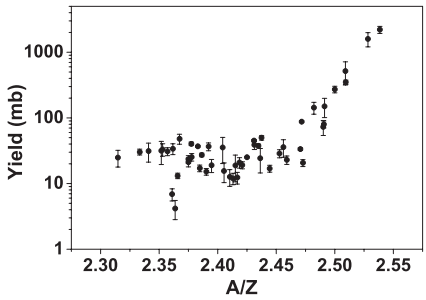

FIG. 3. Plot of mass yields as a function of "A/Z" of the corresponding fission products. The charge distribution correction with the parameters for CFF results in anomalously large mass yields for the fission products with $A/Z \sim > 2.47$.

marks the position of $(A/Z)_p$ obtained from the isotopic yield distribution of Sb as shown in Fig. 1. The right arrow marks the position of $(A/Z)_p$ of 2.52 for TF as obtained from Ref. [19], which almost coincides with the maximum in the yield (independent or nearly independent) distribution for TF. It is also to be noted that some of the fission products in the lower mass region of the mass distribution have their A/Z such that they cannot be separated clearly into CFF or TF products based on A/Z. Also, there can be contribution from TF to the measured yield owing to decay of the precursor with higher A/Z. Hence, the following procedure was adopted for apportioning the yields to CFF and TF.

The relatively neutron deficient nuclides ^{122,124,126}Sb, ^{128,130}I, ^{136}Cs, ^{133}Ba, ^{134}Cs, and ^{150}Pm are presumed to be predominantly formed in CFF. Based on A/Z, values, it can be assumed that ^{141}Ba is predominantly formed in TF while ^{141}Ce and its precursor ^{141}La is mostly formed in CFF. Hence, the cumulative yield of ^{141}Ce, after subtracting the ^{141}Ba cumulative yield is also presumed to be attributable to CFF. The products, ^{78}As and ^{85}Kr^m, will have negligible contribution from TF, as yields from asymmetric fission will be negligible at these mass numbers. The independent/cumulative yields of these 12 fission products originating from CFF were corrected for charge distribution using $\sigma_Z = 0.8$ and $(A_{cn} - \nu_T)/Z_{cn} = 2.418$ to get the corresponding CFF

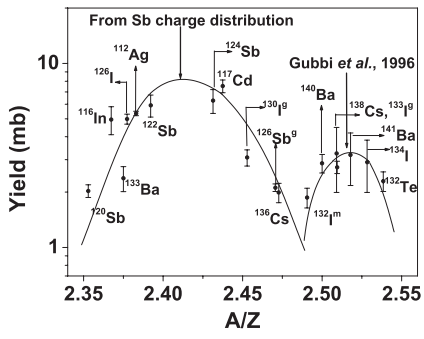

FIG. 4. Plot of independent or nearly independent yields of fission products as a function of their A/Z. Solid lines are guides for the eye. The left downward arrow marks most probable A/Z obtained from the charge distribution of Sb isotopes which corresponds to CFF. The right downward arrow marks the most probable A/Z for TF as given in Gubbi *et al.* 1996 [19].

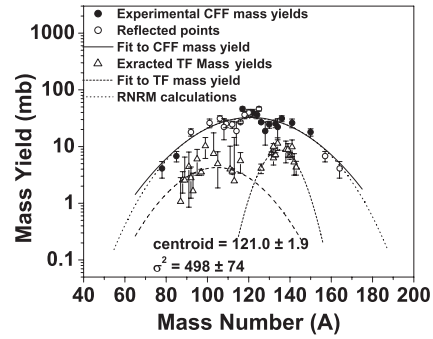

FIG. 5. Plot of mass yields obtained for ^{20}Ne + ^{232}Th reaction at E_{lab} = 142.5 MeV. Solid circles (●) are the experimental CFF mass yields and open triangles (Δ) are the extracted TF mass yields. Open circles (○) are the reflected complementary yields obtained by assigning the experimental mass yield for a mass chain "A" to its complementary mass $A_{comp}(= A_{cn} - \nu_T - A)$, where A_{cn} is the compound nucleus mass number and ν_T is the neutrons lost in the fission process. The solid line is a Gaussian fit to the experimental and complementary yields for CFF. The dotted line is random neck rupture (RNRM) [24,25] calculations. Dashed lines are the Gaussian fits to TF mass yields.

mass yields. The mass yields and the reflected points were best fitted to a Gaussian CFF mass distribution. These mass yields, along with the fitted Gaussian mass distribution, are shown in Fig. 5. The variance of the mass distribution is 498 ± 74. This is in agreement with the reported values for similar systems in the literature [36,37]. The fitted Gaussian gives an estimate of the CFF mass yields (Y_A) of different masses. The cumulative $[CU(A,Z)]$/independent $[IN(A,Z)]$ yields of different fission products formed in CFF were estimated from the CFF mass yields (Y_A) using Eqs. (2) and (3). The estimated yields of the CFF products were subtracted from the experimental cross sections to obtain the cumulative/independent cross sections of the products formed in TF. The estimated TF cross sections are significant for several fission products and require appropriate charge distribution correction to get the mass distribution for the transfer fission component.

Charge distribution parameters for TF were taken from the studies of Gubbi *et al.* [19] on ^{19}F + ^{232}Th reaction. In these studies, fission following proton and α transfer was considered to be the dominant TF contribution. Because the present reaction system is close to ^{19}F + ^{232}Th, the average A/Z of the fissioning nucleus in TF is expected to be similar in both the systems. Owing to the difference in the projectile structure, the relative probability of proton and α transfer may be different in the present reaction compared to that in the ^{19}F + ^{232}Th reaction. However, it is not expected to affect the similarity of A/Z for TF in ^{19}F + ^{232}Th and ^{20}Ne + ^{232}Th reactions as A/Z of the fissioning system formed after proton and α transfer to ^{232}Th nucleus would be similar. Thus, for the charge distribution correction for TF, the $(A/Z)_p$ value was taken as 2.52 from Ref. [19]. The value of σ_Z was taken as 0.7 from Ref. [38]. The resulting mass distribution obtained using the charge distribution parameters for TF is asymmetric.

Fission product mass distributions obtained after using appropriate parameters for charge distribution correction for

CFF and TF are shown in Fig. 5. Mass distributions for CFF and TF are shown as solid circles and open triangles, respectively. As expected, mass distribution is symmetric for CFF, indicating the absence of shell effects owing to higher excitation energy of the fissioning nucleus. The fitted Gaussian distribution is shown as the solid line. From the best fit, the centroid of the mass distribution was obtained as 121.0 ± 1.9, which corresponds to a ν_T value of 10.0 ± 3.8, which is in close agreement with the value used in the calculation of $(A/Z)_p$ [34]. The CFF cross section ($\sigma_{\rm fus}$) obtained from the fitting was 913 ± 64 mb. The quoted uncertainty is the fitting error. Fission cross section was also calculated using the statistical model code PACE2 [39]. In the calculations, compound nucleus l distribution was generated using the code PACE2 (which uses the Bass model [40]) with diffuseness parameter of 0.3. Level density parameter a was taken as $A/8.5$ MeV^{-1}. The ratio a_f/a_n was taken as unity. The code PACE2 uses the finite range fission barrier of Sierk [41] as the default value. The calculated fission cross section at $E_{\rm lab}$ = 142.5 MeV was 921 mb. The experimental fission cross section agrees well with the calculated value. Mass distribution for TF was observed to be asymmetric owing to the lower excitation energy of the fissioning system for TF. This observation was consistent with the earlier studies in the ^{19}F, ^{11}B + ^{232}Th reaction [19,35]. The lighter mass wing of the TF mass distribution is broader than the heavier one, as observed in earlier studies [19,35]. An estimate of the transfer fission cross section was obtained by fitting the separate wings in TF mass distribution to a Gaussian function. TF cross section was obtained as 162 ± 14, which is ∼15% of the total fission cross section at this beam energy.

According to the sumrule model calculations of Wilczynski [42,43], $l_{\rm cr}$ for complete fusion is 56$\hbar$ and $l_{\rm max}$ at this beam energy is 72$\hbar$. Based on these calculations, the total cross section for noncompound processes, i.e., the cross section between $l_{\rm cr}$ and $l_{\rm max}$, is 353 mb. The cross sections of the evaporation residues, ^{232}Pa and ^{233}Pa, formed in proton transfer channels at this beam energy are also listed in Table II. The total cross section of the proton transfer products is 55.1 ± 1.3 mb at $E_{\rm lab}$ = 142.5 MeV and the TFF cross section is 162 ± 14 mb, as mentioned above. Thus, the measured total transfer cross section is less than the calculated value. The remaining cross section may be attributable to the unobserved transfer products mainly formed in α-transfer channels. It should be mentioned here that the fusion cross section calculated by the sumrule model at this beam energy is 1115 mb, whereas the experimental fusion cross section is 913 ± 64 mb and the PACE2 calculation gives 921 mb. This may be attributable to the different value of of radius constant, r_0, used in the sumrule model calculations.

3. *Random neck rupture model calculations*

The variance ($\sigma_A{}^2$) of the mass distribution for CFF was obtained as 498 ± 74, which was in reasonable agreement with the literature values for ^{19}F + ^{232}Th [19], ^{16}O + ^{238}U [36], and ^{20}Ne + ^{232}Th [37] reactions at similar excitation energy of the compound nucleus. In the present work, RNRM [24,25] calculations have been performed to calculate the variance of mass distribution. According to RNRM, mass distribution in the fission process is governed by the pre-scission shape. During the motion of the fissioning nucleus towards scission, a dent is developed in the neck region of the fissioning nucleus, which is deepened by the capillary force, finally leading to fission. The curvature of the fissioning nucleus changes from positive to negative in the motion towards scission. During this transition when the neck becomes flat, there can be a large shift in the dent without sizeable physical mass motion, which finally leads to a large mass fluctuation in fission. In the RNRM model [24,25] the pre-scission shape for the symmetric fission is described by the following set of equations:

$$\rho(z) = \begin{cases} \left(r_1^2 - z^2\right)^{1/2}, & r_1 \leqslant z \leqslant z_1, \\ r_2 + a^2 c\left(\cosh\dfrac{z - d/2}{a} - 1\right), & z_1 \leqslant z \leqslant d - z_1, \\ \left[r_1^2 - (d-z)^2\right]^{1/2}, & d - z_1 \leqslant z \leqslant d + r_1. \end{cases} \quad (9)$$

Equation (9) represents a shape that is made up of two equal spheres which are connected by a neck with minimal curvature c. This shape involves six parameters (r_1, z_1, r_2, a, c, d). r_1 is the radii of the spherical heads of the two halves, c is the curvature of the neck, a is extension of the neck, r_2 is the minimal neck radius, and z_1 is the transitional point where the function describing the shape changes. The total elongation L of the pre-scission shape is $d + 2r_1$. By imposing the conditions of continuity of the shape and volume conservation, a set of nonlinear equations were obtained. The equations were solved using the algorithms from Ref. [44] to determine r_1, z_1, and a. The neck parameter r_2 was fixed by Rayleigh's instability criterion as given by Eq. [25],

$$d - 2\tilde{r}_1 = 4.5 r_2, \quad (10)$$

where $\tilde{r}_1$ was calculated as $1.15(A_{\rm cn}/2)^{1/3}$. The curvature c was calculated using the following equation [25]:

$$c = c_{\rm rel} \cdot 8 \cdot (\tilde{r}_1 - r_2)/d^2. \quad (11)$$

The value of $c_{\rm rel}$ was taken as 0.1 as used in Ref. [25]. The remaining variable d was varied to reproduce the experimental variance of mass distribution. The final value of the elongation parameter d was obtained as 30.29 fm. This value of d was used to calculate the $\overline{\rm TKE}$ using the prescription given in Ref. [25]. The calculated value of $\overline{\rm TKE}$ was found to be 189.7 MeV, which was close to the experimental value for ^{238}U + ^{16}O reaction forming similar compound nucleus [45]. The mass distribution calculated using RNRM is shown in Fig. 5 as a dotted line. The pre-scission shape obtained from RNRM calculations is shown in Fig. 6.

The scission-point elongation can also be obtained from LDM. According to LDM, the scission point is given by the condition [29]

$$\rho_{\rm cm} \approx 1.16 R_0, \quad (12)$$

where $\rho_{\rm cm}$ is half the distance between the centers of mass of the two halves of the nucleus. The quantity "$2\rho_{\rm cm}$", which is similar to d in RNRM, though not exactly the same, was obtained as 16.85 fm. Taking $2\rho_{\rm cm}$ as $d_{\rm LDM}$, the ratio

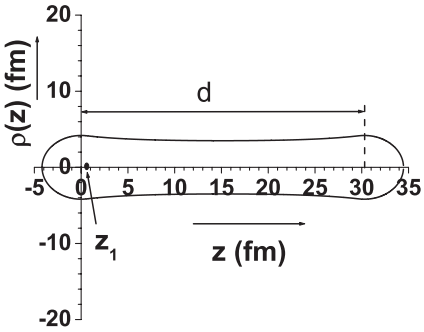

FIG. 6. Pre-scission shape of ^{252}Fm obtained from RNRM [24,25] calculations. Various symbols are defined in the text.

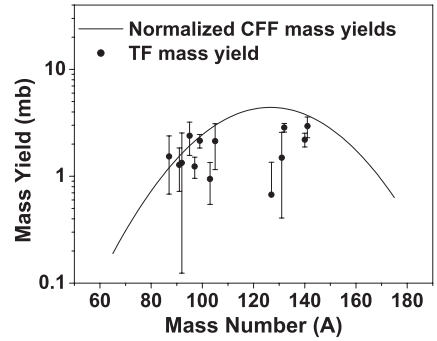

FIG. 7. TFF mass yields at $E_{\rm lab} = 114$ MeV. The solid line is the CFF mass distribution obtained by normalizing the CFF Gaussian fit of higher energy. The details are given in text.

$d_{\rm RNRM}/d_{\rm LDM}$ was obtained as 1.80, which was close to a nearly constant value of 1.76 ± 0.02 obtained from the analysis of the variance data for fissioning systems spanning over a wide range of fissility [26,27].

B. Mass distribution studies at 114 MeV in ^{20}Ne + ^{232}Th reaction

At $E_{\rm lab} = 114$ MeV, the formation cross sections of the fission products were obtained by adding their cross sections in the forward and backward catcher foils and in the target. The formation cross sections of 22 fission products are given in Table II. Owing to the lower fission cross section, the number of fission products whose yield could be determined was much less compared to that at $E_{\rm lab} = 142.5$ MeV. As formation cross section for sufficient number of isotopes for a given Z could not be determined, the σ_Z value of 0.80, obtained at $E_{\rm lab} = 142.5$ MeV, was used at this beam energy for charge distribution correction. This approximation is justified as σ_Z value is nearly constant at moderate excitation energies. As done at $E_{\rm lab} = 142.5$ MeV, the Z_p values for different mass chains were calculated using the UCD hypothesis with $\nu_T = 8.06$ obtained using the prescription of Kozuline *et al.* [34]. The nature of CFF mass distribution at lower beam energy is expected to be similar to that at higher energy. The independent yields of fission products in the symmetric mass region (^{117}Cd, ^{126}Sb^g, and ^{130}I) are expected to have negligible contribution from TF as TF mass distribution is asymmetric. The average ratio of the CFF mass yields from these three fission products at $E_{\rm lab} = 142.5$ and 114 MeV was found to be 7.404. The CFF mass distribution at $E_{\rm lab} = 114$ MeV was obtained by normalizing the CFF mass distribution Gaussian fit at high energy by this factor. Based on this normalization, the CFF cross section at 114 MeV is estimated to be 123 ± 36 mb. The PACE2 calculations predict the fusion cross section as 105 mb, which shows the reasonable agreement between calculated and experimental values. The TF contribution to the experimental yields of the remaining fission products were obtained by adopting a procedure similar to that done at $E_{\rm lab} = 142.5$ MeV. The extracted TF mass yields along with the normalized fitted curve for CFF at $E_{\rm lab} = 114$ MeV are shown in Fig. 7. On comparing Figs. 5 and 7, it can be seen that the TF mass yields are almost comparable to normalized CFF mass yields at lower beam energy, indicating relative contribution of TF increases at lower beam energy. This could be attributable to the rapid fall in CFF cross section with decreasing beam energy than the transfer reaction cross section close to the barrier. The extracted TF mass yields at lower energy are scattered and, thus, could not be fitted to get an estimate of the TF cross section. The total cross section of the evaporation residues formed by proton transfer to the target was measured as 31.6 ± 1.2 (Table II), which is ∼30% of the cross section of CFF ($\sigma_{\rm fus}$). This is higher fraction as compared to 55.1 ± 1.3 mb (∼5% of $\sigma_{\rm fus}$) at $E_{\rm lab} = 142.5$ MeV, indicating a higher transfer fraction. This is consistent with the observed higher cross section for TFF relative to CFF.

IV. CONCLUSION

Fission product mass distribution in ^{20}Ne + ^{232}Th reaction was studied at beam energies of 142.5 and 114 MeV. Experimentally measured yields of fission products were corrected for the charge distribution to obtain the mass yields. The width parameter (σ_Z) required for the charge distribution correction for CFF was obtained using the experimentally measured independent yields of Sb isotopes at 142.5 MeV, which agreed well with the values reported in the literature for similar systems at similar excitation energies. Fission products with $A/Z > 2.47$ were observed to be predominantly produced in transfer-induced fusion fission (TF). The TF mass yields were extracted from the experimental yields by subtracting the CFF contribution. At both beam energies, the mass distributions owing to CFF were observed to be symmetric and those owing to TF were observed to be asymmetric, with a broader, lighter wing. On comparing the mass yields of CFF and TF mass distribution, it was observed that the TF contribution increases with decreasing beam energy. The variance of the mass distribution for CFF was calculated using the RNRM. Scission-point elongation determined from RNRM was observed to be higher than that obtained from LDM potential energy calculation. This observation was consistent with the results of the analysis of variance data over a wide range of fissioning systems.

ACKNOWLEDGMENTS

The authors thank Dr. D. Dutta for his help during the experiment. The authors gratefully acknowledge Dr. A. Goswami, head, Radiochemistry Division, BARC, and Dr. P. K. Pujari, head, Nuclear Chemistry section, RCD, BARC, for their interest and valuable suggestions. Thanks are due to the operating staff of VECC for their cooperation during the experiment.

[1] R. Vandenbosch and J. R. Huizenga, *Nuclear Fission* (Academic Press, New York, 1973).
[2] C. Waggemans, *The Nuclear Fission Process* (CRC, London, 1991).
[3] K. Nishio, H. Ikezoe, S. Mitsuoka, I. Nishinaka, Y. Nagame, Y. Watanabe, T. Ohtsuki, K. Hirose, and S. Hoffmann, Phys. Rev. C **77**, 064607 (2008).
[4] K. Nishio, H. Ikezoe, I. Nishinaka, S. Mitsuoka, T. Ohtsuki, Y. Watanabe, Y. Aritomo, and S. Hofmann, Phys. Rev. C. **82**, 044604 (2010).
[5] M. G. Itkis, I. M. Itkis, G. N. Knyazheva, and E. M. Kozuline, Nucl. Phys. A **834**, 374c (2010).
[6] A. Yu. Chizhov, M. G. Itkis, I. M. Itkis, G. N. Kniajeva, E. M. Kozuline, N. A. Kondratiev, I. V. Pokrovsky, R. N. Sagaidak, V. M. Voskressensky, and A. V. Yeremin, Phys. Rev. C **67**, 011603(R) (2003).
[7] R. Rafiei, R. G. Thomas, D. J. Hinde, M. Dasgupta, C. R. Morton, L. R. Gasques, M. L. Brown, and M. D. Rodrigues, Phys. Rev. C **77**, 024606 (2008).
[8] Appannababu *et al*., Phys. Rev. C **83**, 034605 (2011).
[9] E. Prasad *et al*., Phys. Rev. C **81**, 054608 (2010).
[10] T. K. Ghosh, S. Pal, T. Sinha, S. Chattopadhyay, P. Bhattacharya, D. C. Biswas, and K. S. Golda, Phys. Rev. C **70**, 011604 (2004).
[11] T. Banerjee *et al*., Phys. Rev. C **83**, 024605 (2011).
[12] J. Toke, R. Bock, G. X. Dai, A. Gobbi, S. Gralla, K. D. Hildenbrand, J. Kuzminski, W. F. J. Muller, A. Olmi, and H. Stelzer, Nucl. Phys. A **440**, 327 (1985).
[13] D. J. Hinde, M. Dasgupta, J. R. Leigh, J. P. Lestone, J. C. Mein, C. R. Morton, J. O. Newton, and H. Timmers, Phys. Rev. Lett. **74**, 1295 (1995).
[14] V. S. Ramamurthy *et al*., Phys. Rev. C **32**, 2182 (1985).
[15] B. B. Back, R. R. Betts, J. E. Gindler, B. D. Wilkins, S. Saini, M. B. Tsang, C. K. Gelbke, W. G. Lynch, M. A. McMahan, and P. A. Baisden, Phys. Rev. C **32**, 195 (1985).
[16] D. Vorkapić and B. Ivanišević, Phys. Rev. C **55**, 2711 (1997).
[17] J. V. Kratz, O. Linljenzin, A. E. Norris, and G. T. Seaborg, Phys. Rev. C **13**, 2347 (1976).
[18] V. Zagrebaev and W. Greiner, J. Phys. G **31**, 825 (2005).
[19] G. K. Gubbi, A. Goswami, B. S. Tomar, B. John, A. Ramaswami, A. V. R. Reddy, P. P. Burte, and S. B. Manohar, Phys. Rev. C **53**, 796 (1996).
[20] M. C. Duh, H. Haba, N. Takashi, A. Yokoyama, and T. Saito, Nucl. Phys. A **550**, 281 (1992).
[21] D. J. Hinde, J. R. Leigh, J. J. M. Bokhorst, J. O. Newton, R. L. Walsh, and J. W. Boldeman, Nucl. Phys. A **472**, 318 (1987).
[22] C. F. Tsang and J. B. Wilhelmy, Nucl. Phys. A **184**, 417 (1972).
[23] B. D. Wilkins, E. P. Steinberg, and R. R. Chasman, Phys. Rev. C **14**, 1832 (1976).
[24] U. Brosa and S. Grossmann, Z. Phys. A **310**, 177 (1983).
[25] U. Brosa, S. Grossmann, and M. Andreas, Phys. Rep. **197**, 167 (1990).
[26] R. Tripathi, Ph.D. thesis, Mumbai University, 2008.
[27] R. Tripathi and A. Goswami, in *Proceedings of the DAE Symposium on Nuclear Physics*, edited by R. K. Choudhury, A. K. Mohanty, and S. Santra (Sambalpur University, Orissa, India, 2007), Vol. 52, p. 439.
[28] R. Tripathi and A. Goswami, Eur. Phys. J. A **26**, 271 (2005).
[29] M. Brack, Damgaard Jens, A. S. Jensen, H. C. Pauli, V. M. Strutinsky, and C. Y. Wong, Rev. Mod. Phys. **44**, 320 (1972).
[30] U. Reus and W. Westmeier, At. Data Nucl. Data Tables **29**, 1 (1983).
[31] R. B. Firestone and V. S. Shirley, *Table of Isotopes* (8th ed.), Vol. I and II (John Wiley and sons., New York, 1999).
[32] P. K. Mukhopadhyaya, in *Proceedings of DAE Symposium on Intelligent Nuclear Instrumentation (INIT-2001)*, edited by S. K. Kataria, P. P. Vaidya, P. V. Narurkar, and S. Roy (BARC, Mumbai, India, 2001), p. 307.
[33] H. H. Rossner, J. R. Huizenga, and W. U. Schroder, Phys. Rev. Lett. **53**, 38 (1984).
[34] E. M. Kozuline, A. Ya. Rusanov, and G. N. Smirenkin, Phys. At. Nucl. **56**, 166 (1993).
[35] G. K. Gubbi, A. Goswami, B. S. Tomar, B. John, A. Ramaswami, A. V. R. Reddy, P. P. Burte, and S. B. Manohar, Phys. Rev. C **59**, 3224 (1999).
[36] J. J. Hogan, D. J. Parker, and J. Asher, Z. Phys. A **338**, 325 (1991).
[37] M. G. Itkis, S. M. Luk'yanov, and V. N. Okolovich, Yad. Fiz. **53**, 1195 (1991).
[38] H. Umezawa, S. Baba, and H. Baba, Nucl. Phys. A **160**, 65 (1971)
[39] A. Gavron, Phys. Rev. C **21**, 230 (1980).
[40] R. Bass, Phys. Lett. B **47**, 139 (1973).
[41] Arnold J. Sierk, Phys. Rev. C **33**, 2039 (1986).
[42] K. Siwek-Wilczynska, E. H. du Marchie van Voorthuysen, J. van Popta, R. H. Siemssen, and J. Wilczynski, Phys. Rev. Lett. **42**, 1599 (1979).
[43] J. Wilczynski, K. Siwek-Wilczynska, J. Van Driel, S. Gonggrijp, D. C. J. M. Hageman, R. V. F. Janssens, J. Lukasiak, R. H. Siemssen, and S. Y. Van Der Werf, Nucl. Phys. A **73**, 109 (1982).
[44] W. H. Press, S. A. Teukolsky, W. T. Vellerling, and B. P. Flannery, *Numerical Recipes in FORTRAN*, 2nd ed. (Cambridge University Press, Cambridge, 1992).
[45] W. Q. Shen *et al*., Phys. Rev. C **36**, 115 (1986).